Oxidation Behavior and Structure Stability at 1250 °C of Chromium-Rich TaC-Containing Cast Alloys Based on Nickel and Cobalt

PATRICE BERTHOD, JEAN-PAUL K. GOMIS, and GHOUTI MEDJAHDI

In this work, six refractory nickel and cobalt-based cast alloys, rich in chromium and designed to be strengthened by tantalum carbides, were cast in controlled atmosphere. Samples were especially prepared to investigate their surface behavior in synthetic air at 1250 °C for three days. Their oxidized states were first characterized by X-ray diffraction (XRD) and scanning electron microscopy (SEM) on surface, prior to following metallography processing. Second, oxides and subsurfaces were examined by SEM and energy dispersion spectrometry (EDS) on cross sections. Results show that the surface and subsurface deterioration by oxidation clearly depend on the relative quantities in Ni and Co in the chemical composition of the alloys. All alloys well-resisted oxidation due to their chromium contents, but beginnings of catastrophic oxidation were noticed for the alloys containing much more cobalt than nickel. Tantalum, present with particularly high contents, played an important role in the oxidation phenomena and for the microstructure stability at elevated temperature. It notably influenced the adherence of the external scale and led to highly stable heat-resistant TaC carbides, the fraction of which is governed by the base element.

https://doi.org/10.1007/s11661-020-05828-8

I. INTRODUCTION

NICKEL and cobalt were with iron the first metals to play the role of base elements for the metallic alloys considered for the manufacturing of components destined to work at high temperature in severe conditions of mechanical stresses and chemical aggressiveness that these components may encounter in service.[1] Chromium was also often present in the chemical compositions of these alloys to form carbides for resisting creep and to allow developing external oxide scales to resist oxidation by gases and corrosion by melts.[2] The polycrystalline and equiaxed microstructures of conventionally cast nickel alloys and cobalt alloys allowed them demonstrating very interesting behavior at high temperature in the mechanical field.[3] Although advanced superalloys with very particular microstructures[4] appeared more or less recently—such as single-crystalline alloys or Oxide Dispersion Strengthened alloys[5]—polycrystalline cast alloys reinforced by carbides remain a good choice for many high-temperature applications requiring chromium for combatting hot corrosion.[6] The best alloys of this category are often designed to contain MC carbides instead of chromium carbides. This is true for nickel-based alloys[7–10] as well as for cobalt-base alloys.[11,12] Although they know morphological changes during long exposures at elevated temperatures,[13–15] the MC carbides evolve slower than chromium carbides in the same conditions. This is the case for cobalt-based alloys containing 30 wt pct Cr and TaC or HfC, but less for alloys reinforced by NbC.[16] The HfC carbides are particularly morphologically stable at elevated temperature in chromium-rich nickel-based[17] and cobalt-based[18] cast alloys, but this is much less true in iron-based alloys.[19,20] However, taking into account both the cost and availability of hafnium, tantalum may be preferred to form highly stable MC carbides.

Great quantities of TaC carbides were present as fibers in the *in situ* composite superalloys, based on nickel[21] or on cobalt[22] which were developed fifty years ago. With lower contents, TaC is present as a constituent of an interdendritic eutectic compound in the equiaxed Mar-M509 cobalt-based superalloy[1,3,23] in which its morphology is Chinese script, besides the chromium carbides also present in the microstructure. More recent alloys rich in chromium containing TaC as single carbide phase present demonstrated melting start temperatures higher than 1300 °C[24] and high creep

PATRICE BERTHOD is with the Université de Lorraine, CNRS, IJL, 54000 Nancy, France. Contact e-mail: patrice.berthod@univ-lorraine.fr JEAN-PAUL K. GOMIS is with the Université de Lorraine, FST, 54500 Vandoeuvre-lès-Nancy, France. GHOUTI MEDJAHDI is with the Université de Lorraine.
Manuscript submitted February 10, 2020.
Article published online May 23, 2020

resistance at 1200 °C.[25] The use of such alloys at temperatures above 1200 °C may be envisaged in case of low level of stresses applied but one can fear that catastrophic oxidation happens after only a few hours.

The objective of this study is to test in oxidation at a temperature higher than 1200 °C, for rather long duration, several nickel-based and cobalt-based alloys rich in chromium and containing quantities of tantalum and carbon in proportions rated to obtain many TaC carbides. The compositions chosen for the alloys are defined to obtain Co/(Ni + Co) relative amounts extended from 0 to 1 with regularly distributed values. The chromium content, which must be high enough to favor a chromia-forming behavior but which must be not too high to avoid significant decrease in melting start temperature, was fixed at 25 wt pct C. Since it was earlier observed that 0.4 wt pct C and 6wt pct Ta were efficient to obtain, in a cobalt-based cast alloy, script-like TaC carbides in the interdendritic spaces and in quantities leading to a good compromise between creep resistance and toughness, these values were kept for the alloys of the present study. So, six alloys, all containing 25Cr-0.4C-6Ta (wt pct) with a Co content increasing progressively from 0 to about 69 wt pct and a Ni content decreasing in the opposite way, were exposed to synthetic air for chosen temperature and duration taken equal to 1250 °C and 70 hours, respectively.

II. EXPERIMENTAL

Elaborated from pure elements (Alfa Aesar, purity > 99.9 wt pct) using a high-frequency induction furnace (CELES, France) in an inert gaseous environment (300 millibars of pure Argon), six ovoid ingots were obtained (weight of each: close to 40 g). These ingots were cut to obtain first samples for the control of the as-cast microstructures and of the chemical compositions, and second flat parts for carrying out the oxidation test.

The parts destined to the alloy characterization in the as-cast state were embedded in a cold resin mixture (ESCIL, France) and ground with SiC papers from #240 to #1200. After their intermediate ultrasonic cleaning, final polishing of the embedded samples was performed with textile disk enriched with 1 μm hard particles.

The parts destined to the oxidation tests were ground with #1200 SiC papers, on their main faces as well as on their edges and corners to smooth them. These parts were placed in a resistive furnace continually crossed by a flow of synthetic air (80 pct N_2-20 pct O_2, all impurities such as water vapor being in extremely low quantities; flow: about 1.5 L/h). The heating was done at a constant rate equal to 20 °C/min, the isothermal stage at 1250 °C during 70 hours, and the cooling rate at 5 °C/min. The six samples were extracted from the cold furnace and subjected to X-ray diffraction to specify the oxides present on their surfaces.

Thereafter a thin gold layer was deposited by cathodic pulverization (JEOL JFC-1200) onto the surfaces of the oxidized samples. The oxidized surfaces were examined with a Scanning Electron Microscope (JEOL, JSM-6010LA) in the Secondary Electrons mode (SEM/SE). Some spot analyses by Energy Dispersion Spectrometry (SEM/EDS) were attempted on some rare regions obviously flat and perpendicular to the electron beam. Results were corrected from the gold contribution. X-maps were also carried out. After these preliminary investigations, resin-embedding, cross-sectional cutting, and grinding/polishing until mirror-like state were carried out, done as previously described for the as-cast metallographic samples.

The as-cast microstructures of the alloys were observed using the SEM in Back Scattered Electrons mode (SEM/BSE) and the chemical compositions of the alloys were controlled by EDS (except carbon). The cross sections were observed with the SEM in BSE mode to visualize the external and internal oxides. These oxides were specified by EDS spot analyses. The same technique was used to obtain concentration profiles from the oxidation front to the bulk, perpendicularly to the oxide scale/alloy interface. The depths of the internal alloy zone affected by oxidation were measured.

III. RESULTS

A. *Characteristics of the Elaborated Alloys*

The embedded and polished samples for the as-cast state characterization were analyzed by SEM/EDS. Globally, the wished chemical compositions were obtained, as shown by the weight content values displayed in Table I. The full frame ×250 analyses performed on five randomly selected locations led to the presented average and standard deviation values. The standard deviations were all lower than 1wt pct, the uncertainty of EDS analysis; consequently, 1 wt pct

Table I. Chemical Compositions of the Obtained Alloys (Average Value ± Standard Deviation, Calculated from at Least Five SEM/EDS ×250 Full Frame Analyses; All Contents in Wt Pct); *Real Carbon Contents Not Measured but Considered as Very Close to the Wished Values

Alloys	0Co-69Ni-Ta	14Co-55Ni-Ta	7Co-42Ni-Ta	42Co-27Ni-Ta	55Co-14Ni-Ta	69Co-0Ni-Ta
Cr	26 ±1	26 ±1	25 ±1	26 ±1	26 ±1	25 ±1
Co	/	13 ±1	26 ±1	41 ±1	53 ±1	67 ±1
Ni	66 ±1	53 ±1	39 ±1	26 ±1	13 ±1	/
Ta	8 ±1	8 ±1	10 ±1	8 ±1	8 ±1	8 ±1
C*	0.4	0.4	0.4	0.4	0.4	0.4

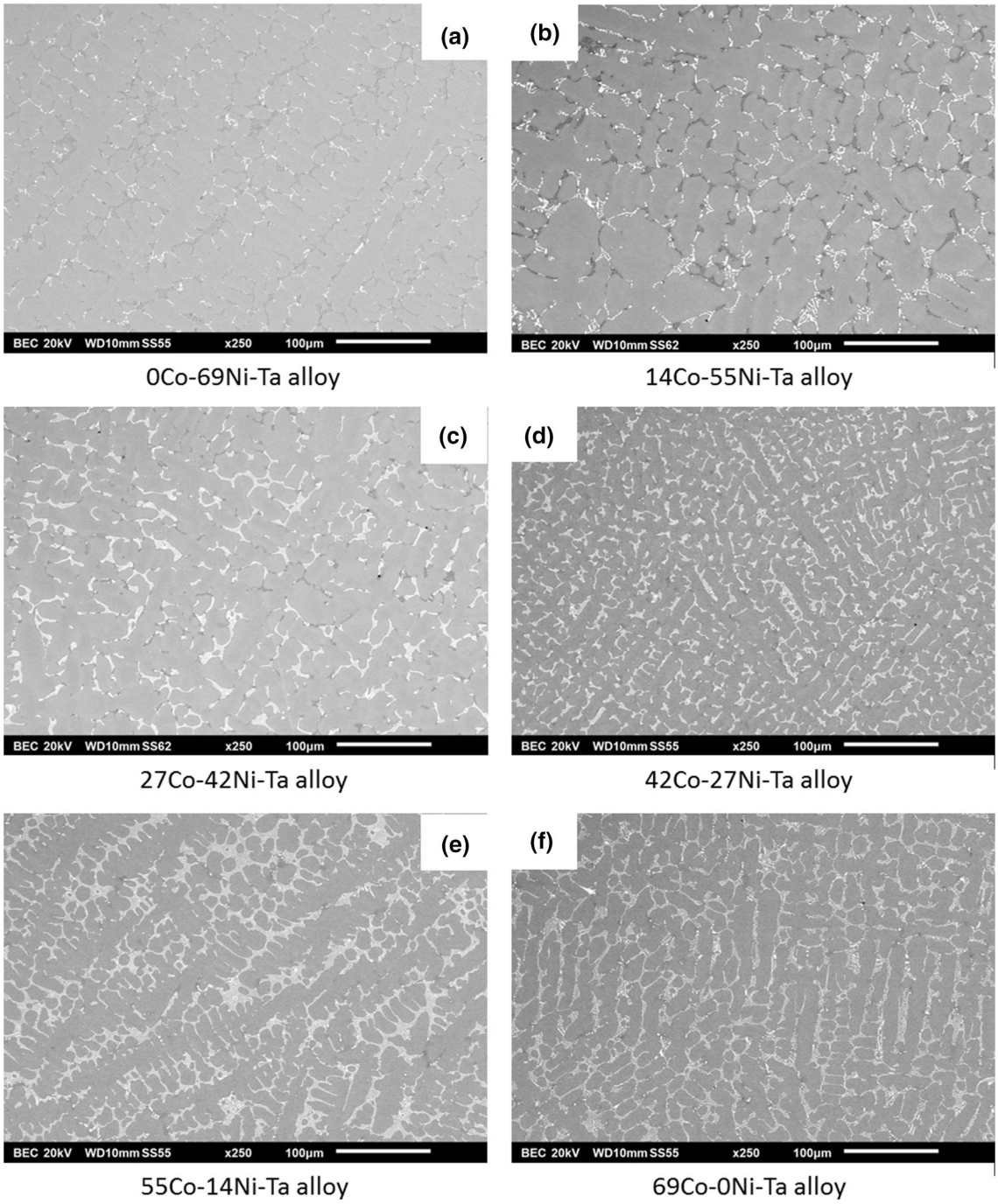

Fig. 1—The as-cast microstructures of the six alloys of the study (SEM/BSE, general view: ×250); (*a*) 0Co-69Ni-Ta, (*b*) 14Co-55Ni-Ta, (*c*) 27Co-42Ni-Ta, (*d*) 42Co-27Ni-Ta, (*e*) 55Co-14Ni-Ta, (*f*) 69Co-0Ni-Ta.

was kept for the uncertainty value. Concerning the average values, one can see that the alloy contents in chromium were well respected. The tantalum contents are obviously overestimated by EDS analysis: this is due to particular distribution of Ta in the alloys: the main part of tantalum is concentrated in the TaC carbides and these ones emerge a little out of the polished surface. This overestimation of Ta logically led to a little underestimation of nickel and cobalt. The carbon content cannot be measured by EDS but, taking into account the obtained carbide fractions, one can guess that the wished C contents were also successfully obtained. One must mention here that the whole elaboration procedure is identical to the ones recently followed for elaborating other alloys of the same category and with similar carbon contents, for which controls of composition by spark spectrometry demonstrated that the obtained contents in carbon (and also in tantalum) are finally very close to the targeted ones.

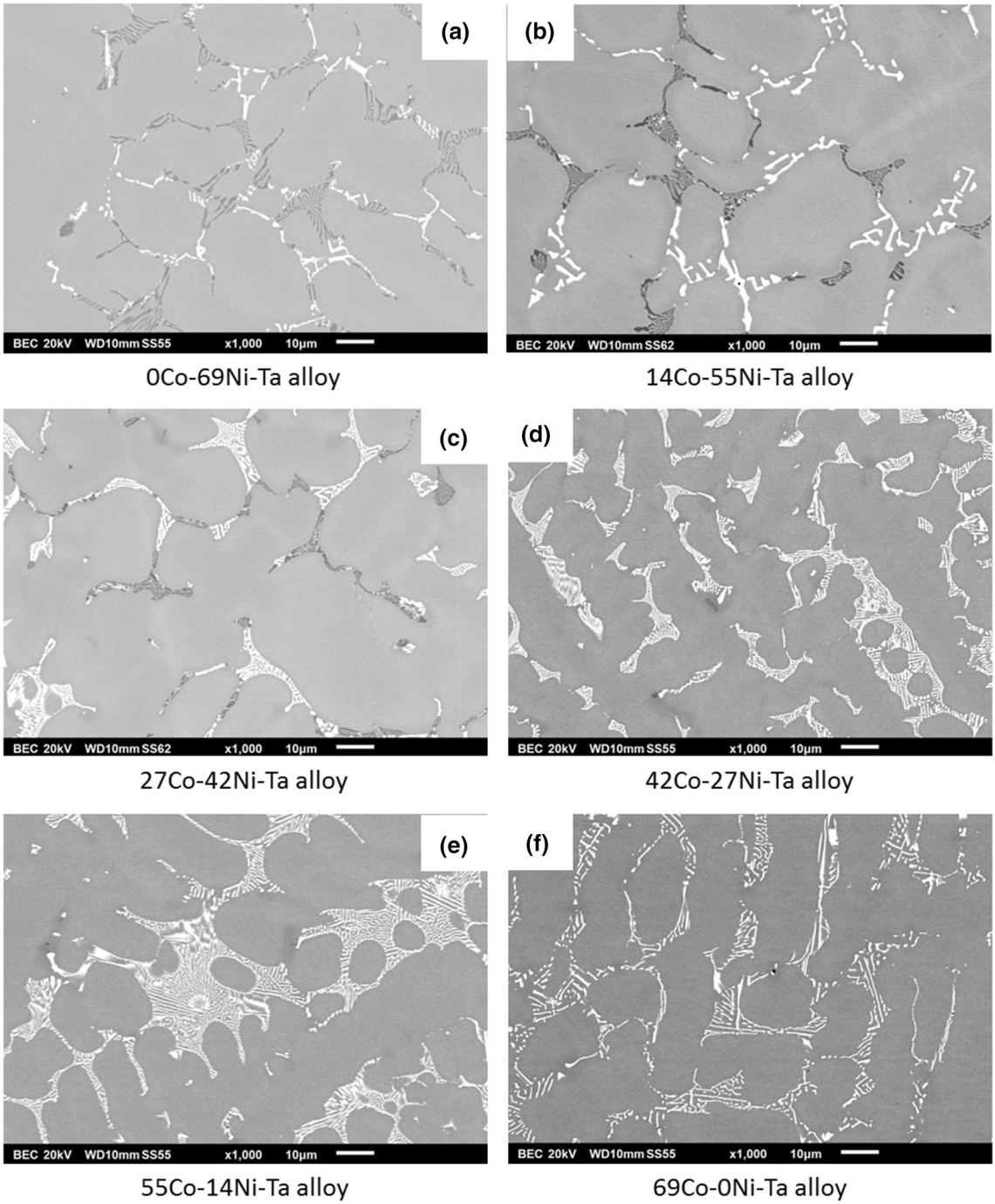

Fig. 2—The as-cast microstructures of the six alloys of the study (SEM/BSE, detailed view: ×1000); (*a*) 0Co-69Ni-Ta, (*b*) 14Co-55Ni-Ta, (*c*) 27Co-42Ni-Ta, (*d*) 42Co-27Ni-Ta, (*e*) 55Co-14Ni-Ta, (*f*) 69Co-0Ni-Ta.

A general view of the as-cast microstructures of the six alloys is given in Figure 1. One can see that all the alloys matrixes are dendritic. It can be seen also that the other phases can be of two natures and that they are necessarily located in the interdendritic spaces in the whole microstructure. The more magnified SEM/BSE micrographs displayed in Figure 2 allow distinguishing the morphologies of the interdendritic phases. The three nickel-richest alloys (named "0Co-69Ni-Ta," "14Co-55Ni-Ta," and "27Co-42Ni-Ta") contain a double carbide population: eutectic chromium carbides (black acicular component of one of the two double-phased interdendritic compounds) and eutectic tantalum carbides (white script-like component of the other double-phased interdendritic compounds). The natures of these two phase were confirmed by spot analysis on the coarsest particles found in each sample): the Cr/C molar ratio of the black phase is close to the one of the Cr_7C_3 carbide and the Ta/C molar ratio of the white phase is close to the one of the TaC monocarbide. One

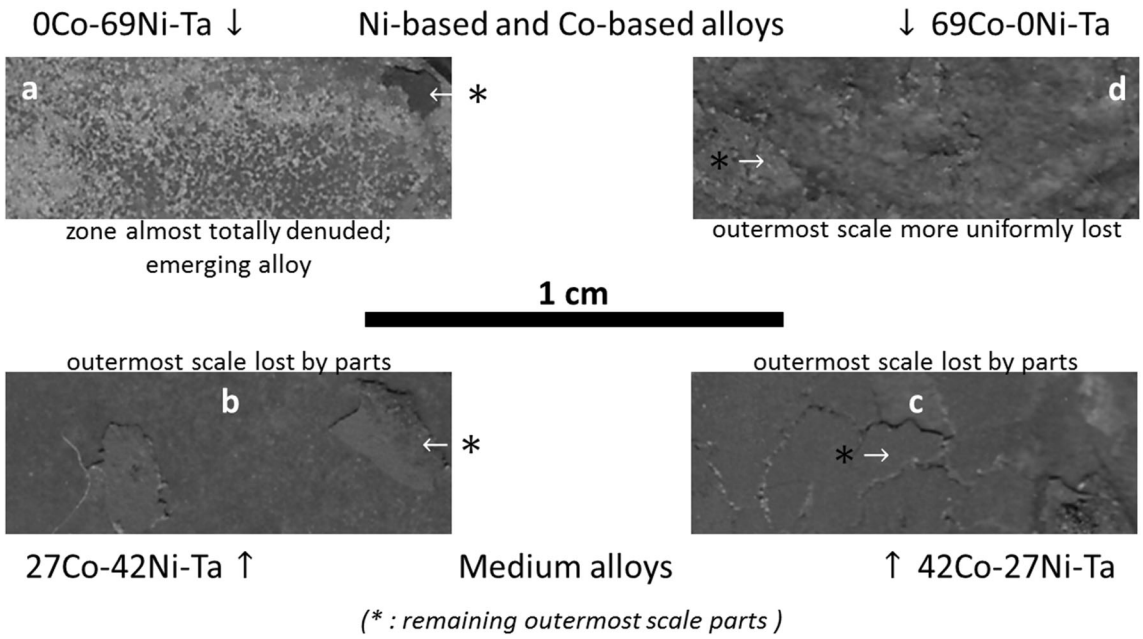

Fig. 3—Oxide spallation states as appearing on photographed surfaces of selected oxidized samples (the two ones based either on Ni (a – 21 mg/cm^2) or Co (d – 85 mg/cm^2) and the two medium alloys (b – 26 mg/cm^2) and (c – 85 mg/cm^2).

must mention here that the used EDS device is able to give accurate values of the carbon content on particles coarse enough and rich enough in carbon, as is was the case for the carbides which were analyzed.

Chromium carbides are much rarer in the three cobalt-richest alloys. These alloys contain TaC as single carbide present.

B. *Oxidized States of the Samples as Characterized Prior to Cross-Sectional Preparation*

Observed with the naked eye it appears that the oxidized surfaces of the samples have lost almost all or at least significant parts of their outermost oxide scales. This is illustrated in Figure 3 by macrophotographs taken on four of the oxidized samples. This is confirmed first by the negative variation of mass per surface unit area between the initial samples and the oxidized ones, for example – 21 and – 85 mg/cm^2 for the 0Co-69Ni-Ta and 69Co-0Ni-Ta alloys, respectively. This also explains the oxides parts found in the neighborhood of each sample when opening the furnace after return to ambient temperature.

The two main faces of each of the six samples were subjected to X-ray diffraction. The two XRD diffractograms acquired on the two faces of a same sample are consistent. For each alloy, only one of them is given. The two XRD diffractograms presented in Figure 4 correspond to the two nickel-richest alloys. The ones given in Figure 5 concern the two intermediate alloys (*i.e.*, with Ni and Co contents close to one another). The ones given in Figure 6 correspond to the two cobalt-richest alloys. The information provided by these XRD diffractograms can be summarized as follows:

- The main oxide detected on the three nickel-richest alloys (Figure 4 and first diffractogram of Figure 5) is the complex oxide of chromium and tantalum, $CrTaO_4$; by increasing the Co content in this series of three alloys, chromia (Cr_2O_3) is more and more present; the diffraction peaks of matrix are particularly intense.
- When cobalt becomes more present than nickel, the spinel oxide $CoCr_2O_4$ appears and co-exists with chromia and $CrTaO_4$; at the same time the matrix diffraction peaks become less and less high (Figures 5 and 6).
- For the two cobalt-richest alloys (Figure 6), cobalt oxide appears in addition to the spinel $CoCr_2O_4$, chromia, and the mixed oxide $CrTaO_4$.

After gold deposition, the oxidized surfaces were observed using the electron microscope in secondary electrons mode. General observation allows seeing that many areas of the surfaces of the three nickel-richest alloys have lost the oxide scale which formed during the high temperature exposure, and that the complex oxide $CrTaO_4$ is the most present oxide on the surface (Figure 7). Denuded alloy is less common on the surfaces of the three cobalt-richest alloys (Figure 8), while chromia and the spinel oxide are often seen (attempts of identification by EDS when possible). Some X-maps were acquired on the oxidized surfaces for completing the characterization. Two examples are showed in Figure 9 (0Co-69Ni-Ta alloy) and in Figure 10 (69Co-0Ni-Ta alloy). The first one allows clearly distinguishing the $CrTaO_4$ oxide covering a part of surface as well as areas of denuded alloy. On the second one, a part of Cr_2O_3 scale and an area of denuded alloy are evidenced.

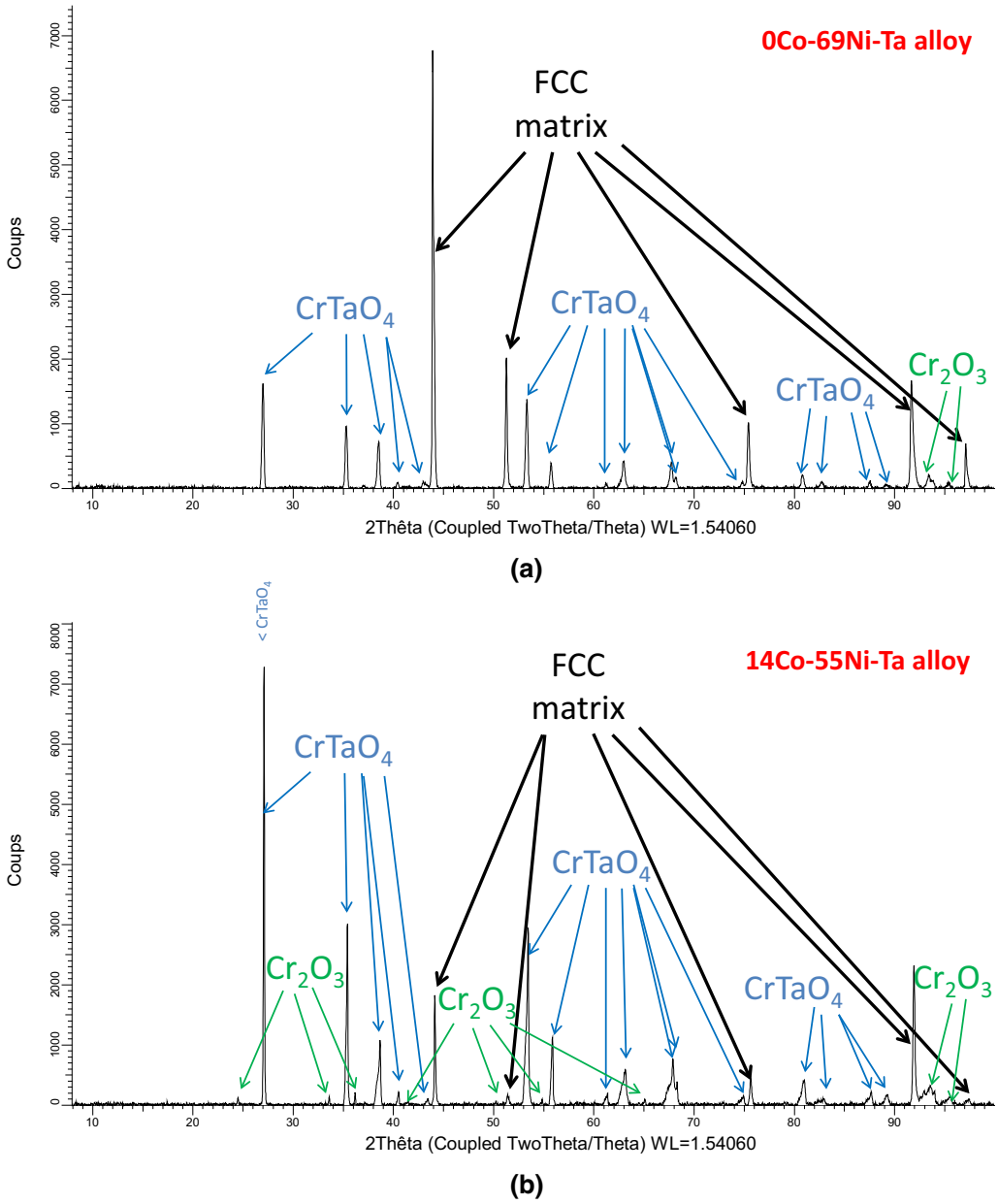

Fig. 4—X-ray diffractograms acquired on the oxidized surfaces of the samples (for the two Ni-based alloys: (*a*) 0Co-69Ni-Ta, (*b*) 14Co-55Ni-Ta).

C. *Oxidized States of the Samples as Characterized on Cross Sections*

The surface states and the internal oxidation in subsurface as observable in cross section are illustrated in Figure 11 by one ×1000 SEM/BSE micrograph per alloy for the four Ni-richest alloys. Obviously the outermost oxides scales suffered intense spallation during the cooling. Oxide scale spallation was particularly severe for the Ni-richest alloys, while more and more external oxides remained on the surface when more and more cobalt was present in the alloy. The oxide which is the more present is the complex oxide of chromium and tantalum $CrTaO_4$.

It is mainly present as more or less interconnected subcortical islands, but some $CrTaO_4$ films can be observed in the parts of external scales that remained on the alloy surface, immersed in chromia. The external scales formed on the surfaces of the two Co-richest alloys remained more efficiently on surface (Figure 12). This allows noticing that the scales (Figure 12 top) can be rather thick (several tens of μm) and that they may contain spinel oxide ($CoCr_2O_4$) and even cobalt oxide. $CrTaO_4$ is also present in great quantity in the outermost part of the subsurface (Figure 12 bottom). In some locations, oxidation has obviously progressed inwards for these two cobalt-richest alloys (Figure 12 right bottom).

The enlarged views ×250 presented in Figure 13 allow observing a phenomenon of disappearance of carbides (chromium carbides for the Ni-richest alloys and tantalum carbides for all alloys). The depth of

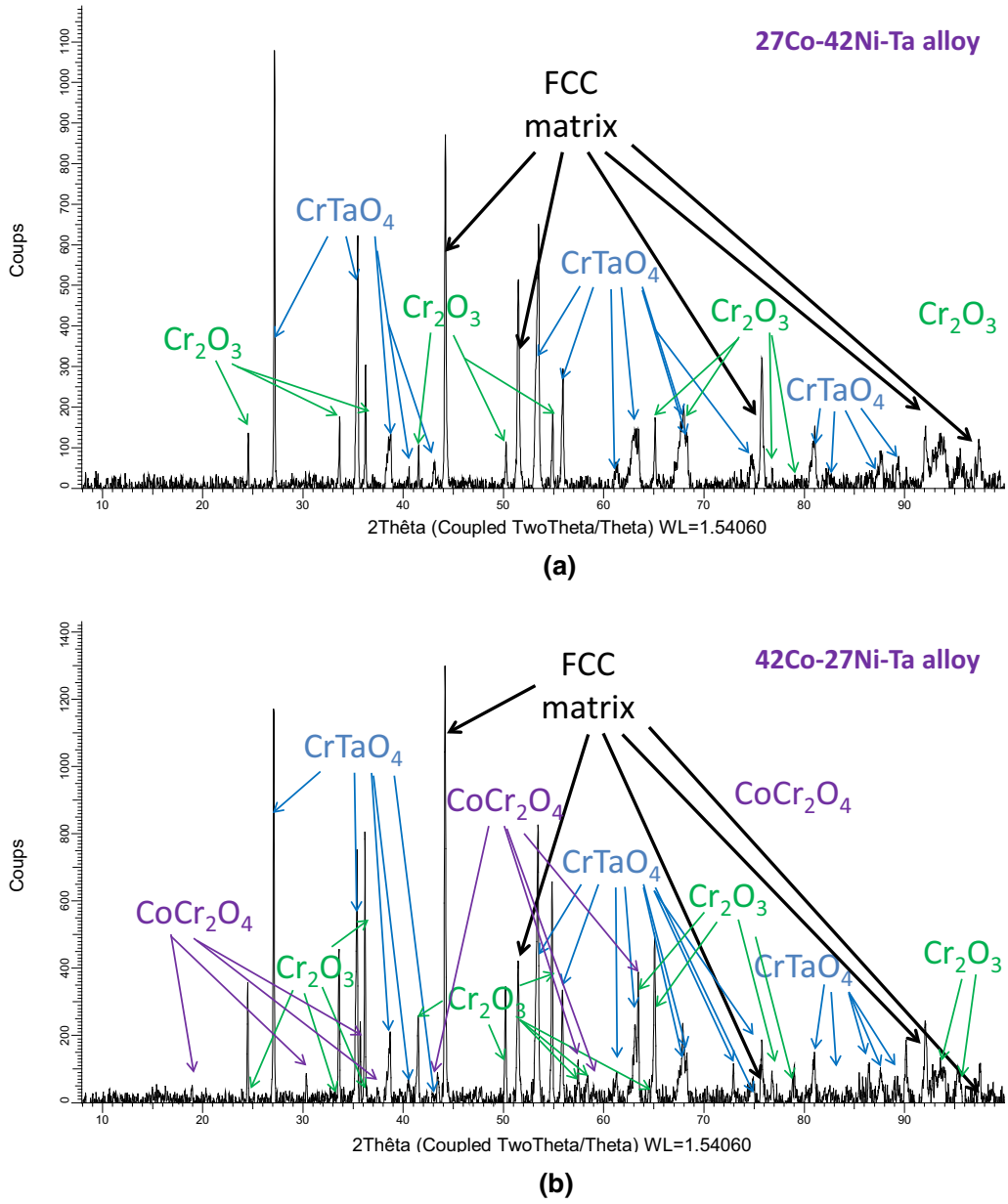

Fig. 5—X-ray diffractograms acquired on the oxidized surfaces of the samples (for the two medium alloys: (*a*) 27Co-42Ni-Ta, (*b*) 42Co-27Ni-Ta).

carbide disappearance tends increasing from the Co-richest alloys to the Ni-richest alloys. The average depths of the carbide-free zones of alloys were measured (ten depth values per alloy) and the results are presented graphically in Figure 14. For the two Ni-richest alloys, the disappearance of the chromium carbides occurred deeper than for the tantalum carbides (about 270 μm against 170 μm). Concerning the other alloys, which only contained initially TaC as carbide phase, they were not concerned by the chromium carbide disappearance. About the tantalum carbides which concerned all the six alloys, one can confirm that the TaC-disappearance depth is deeper for the Ni-richest alloys than for the Co-richest ones. Furthermore, the TaC-depleted depth regularly decreases from the 0Co-69Ni-Ta alloy ($\approx$ 180 μm) to the 69Co-0Ni-Ta alloy ($\approx$ 120 μm).

Spot EDS concentration profiles were acquired from the oxide scale/alloy interface inwards the bulk. The obtained profiles are displayed in Figure 15 for the three Ni-richest alloys and in Figure 16 for the three Co-richest alloys. Concerning chromium, the depth of chromium depletion is seemingly the same for all alloys (between 250 and 300 μm). This depth is similar to the depth of disappearance of the chromium carbides for the two nickel-richest alloys. Such comparison cannot be done for the other alloys since they did not contain this type of carbide (or in much lower quantity, case of the 27Co-42Ni-Ta alloy). The differences concerning the chromium profiles existing between the six alloys are to

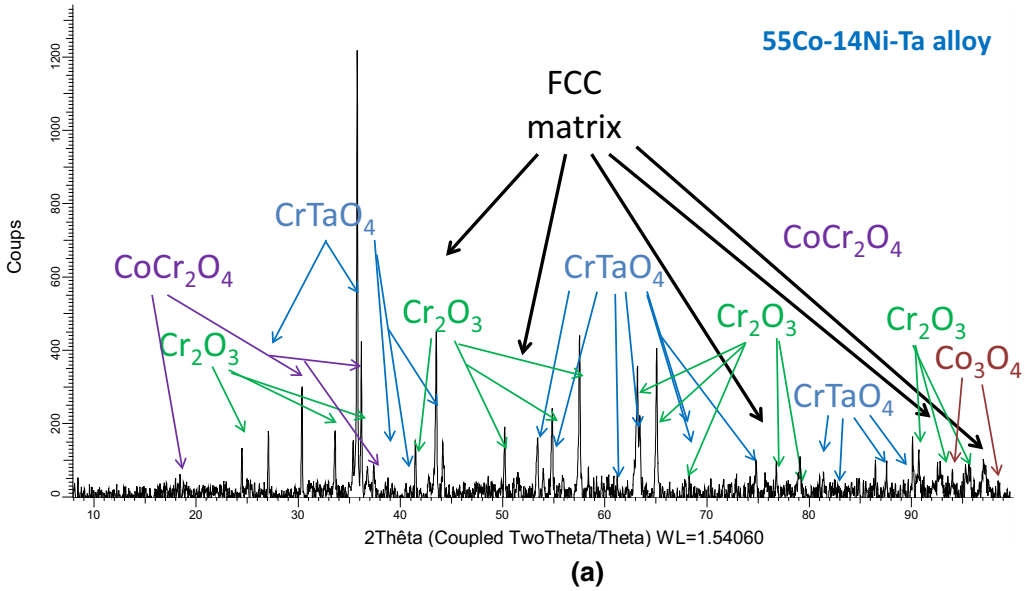

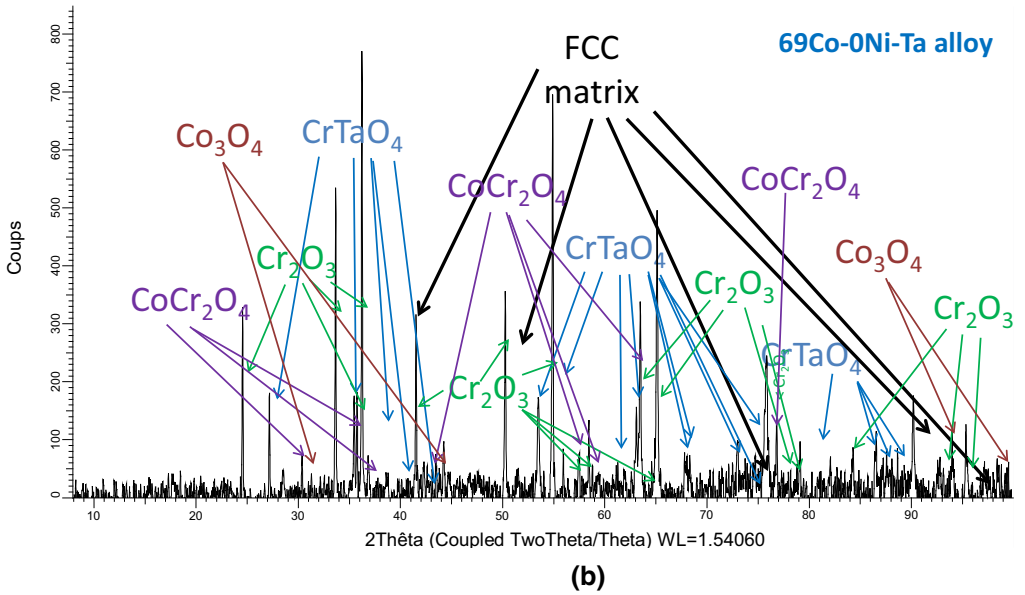

Fig. 6—X-ray diffractograms acquired on the oxidized surfaces of the samples (for the two Co-based alloys: (*a*) 55Co-14Ni-Ta, (*b*) 69Co-0Ni-Ta).

be found in the outermost part of the subsurface: when the alloy contains more and more cobalt and less and less nickel, the chromium content in extreme surface progressively decreases, from about 18 wt pct to about 12 wt pct. Logically, the average chromium content gradient becomes higher and higher. This increase in Cr gradient suggests that the diffusion of chromium toward the oxidation front becomes more and more difficult. Concerning tantalum one can see, in the same time, a decrease in Ta content. This may be due too to more and more difficult diffusion of tantalum, to be oxidized in $CrTaO_4$ on surface or very close to the extreme surface (as seen during the cross-sectional observations). This decrease in Ta content in extreme surface when more and more cobalt is present in alloy at the expense of nickel can be also due to the initially high Ta concentration in the matrix of the nickel-richest alloys existing consequently to the lower implication of Ta in forming carbides in their case.

D. *Microstructures Changes in the Bulk Due to the 70 Hours Stay at 1250 °C*

The bulk microstructures of the alloys after the exposure at high temperature are illustrated in Figure 17 (low magnification, general view) and in Figure 18 (higher magnification, detailed view). The natures, locations, and volume fractions of carbides seem to be similar to the initial ones. In contrast, their morphologies have obviously underwent coarsening

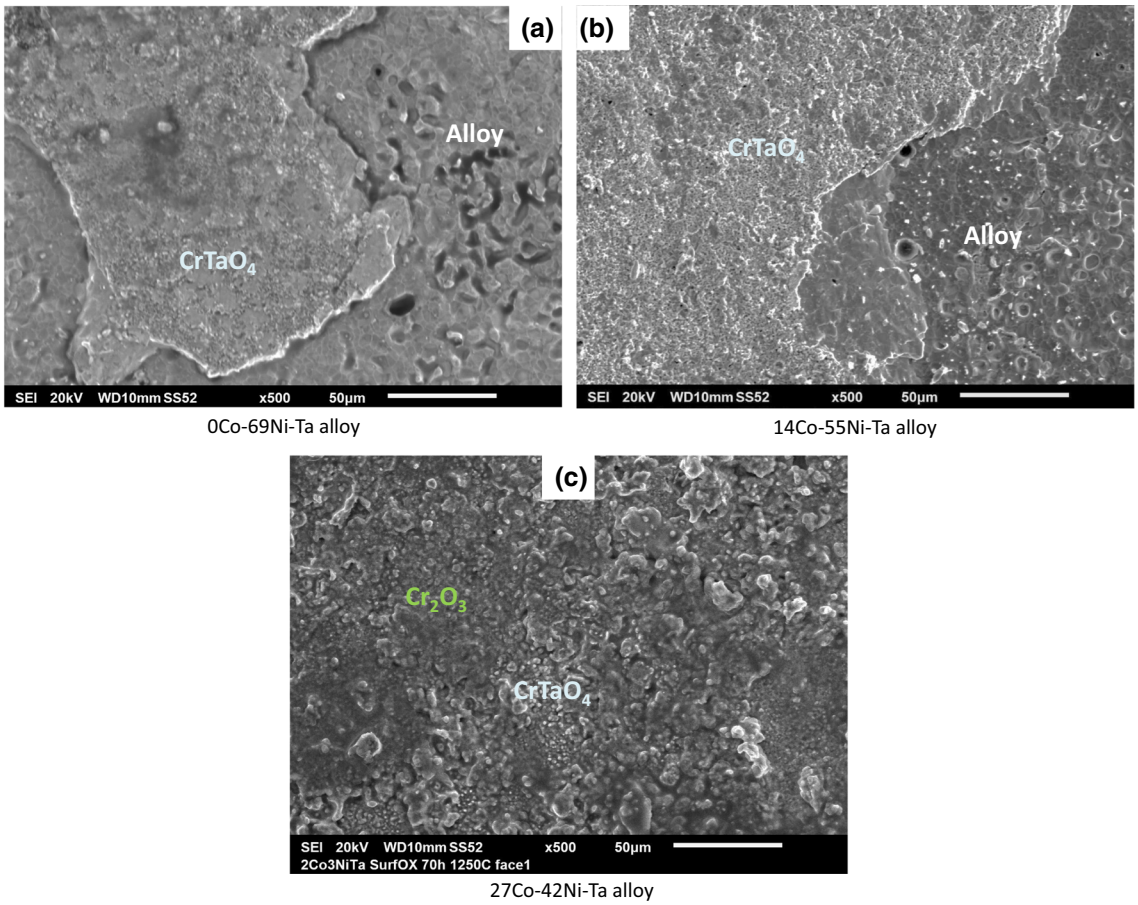

Fig. 7—Aspect of the oxides staying on surface and of the parts of the alloys denuded by spallation (for the three Ni-richest alloys: (*a*) 0Co-69Ni-Ta, (*b*) 14Co-55Ni-Ta, and (*c*) 27Co-42Ni-Ta; SEM/SE, ×500).

and/or fragmentation. The chromium carbides of the three nickel-richest alloys have lost their acicular shape, inherited from the process of the eutectic solidification, and they get coalesced and coarsened. The tantalum carbides of all alloys also evolved in morphology: the script-like carbides became fragmented but their coalescence and coarsening were less achieved than in the case of the chromium carbides.

IV. DISCUSSION

Despite the low quantities of alloys (ingots of about 40 g), the targeted contents in all elements were successfully obtained, thanks to the pure argon atmosphere at the pressure of several hundreds of millibars which allowed limiting oxidation and gaseous species formation. This verdict let us think that no not-melted parts exist in the ingots, as also suggested by the visual observation of the surfaces of all cut samples. The observed microstructures of the as-cast alloys show that solidification started by the crystallization of the FCC solid solution, with a dendritic shape. The interdendritic residual liquid solidified as eutectic {FCC matrix + carbides} compounds: {FCC matrix + Cr_7C_3 + TaC} ternary eutectics for the three nickel-richest alloys, and {FCC matrix + TaC} binary eutectics for the three cobalt-richest alloys. Thus, no pre-eutectic carbides precipitated prior to the matrix dendrite development, for all alloys. These ones are therefore free of too coarse chromium carbide or tantalum carbides which may threaten first the mechanical resistance at high temperature and second the hot oxidation behavior by possibly disturbing locally the expected chromia-forming behavior because of a too high concentration of highly oxidable element.

All carbides are thus obviously of a eutectic nature and well distributed in the interdendritic spaces where they may consolidate the dendritic structure for efficiently resisting stresses as well as the third stage of creep. However, the presence of eutectic compounds can lead to lowered refractoriness. Fortunately, for all alloys the exposures at 1250 °C did not induce any local melting as evidenced during the bulk examination of the aged alloys, even for the three nickel-richest alloys in which eutectic chromium carbides were present together with the tantalum carbides.

Melting did not occur in alloys during the tests at 1250 °C, but this temperature was obviously too high for the morphologic stability of the carbides, especially

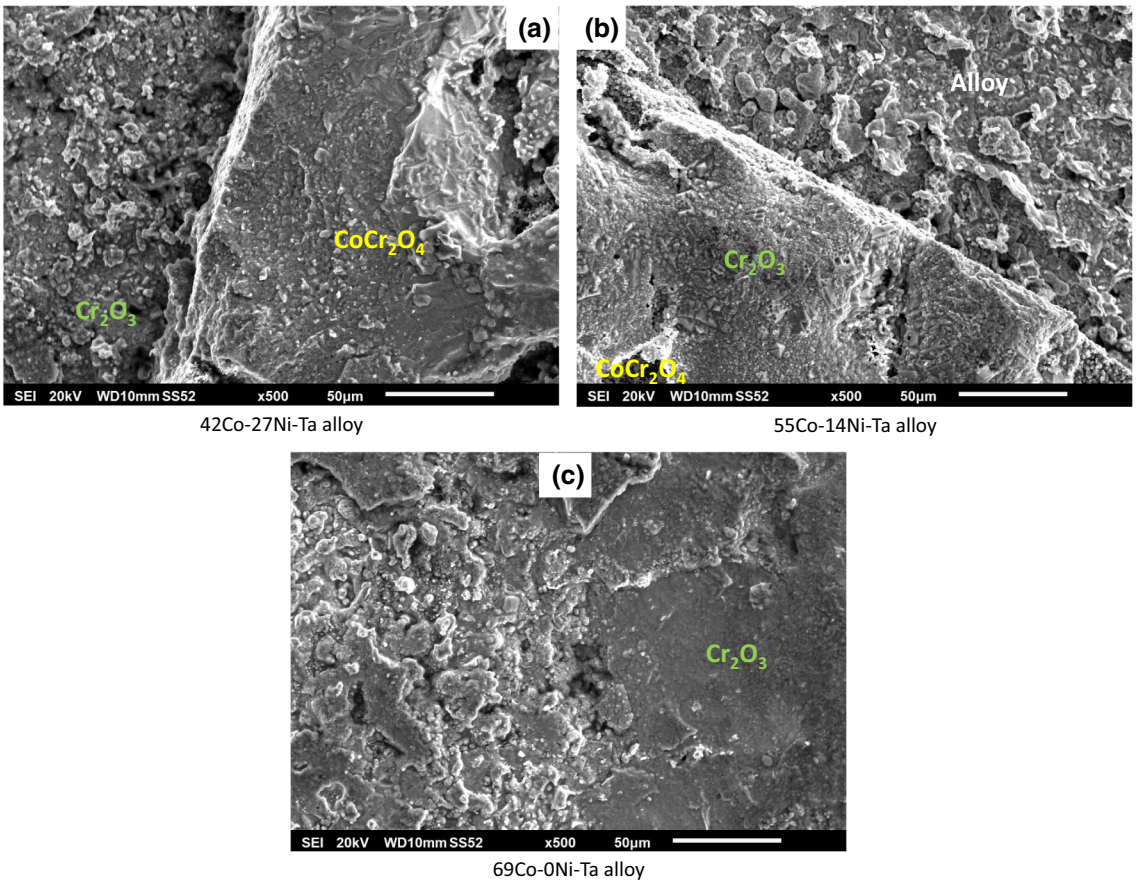

Fig. 8—Aspect of the oxides staying on surface and of the parts of the alloys denuded by spallation (for the three Co-richest alloys: (*a*) 42Co-27Ni-Ta, (*b*) 55Co-14Ni-Ta, and (*c*) 69Co-0Ni-Ta; SEM/SE, ×500).

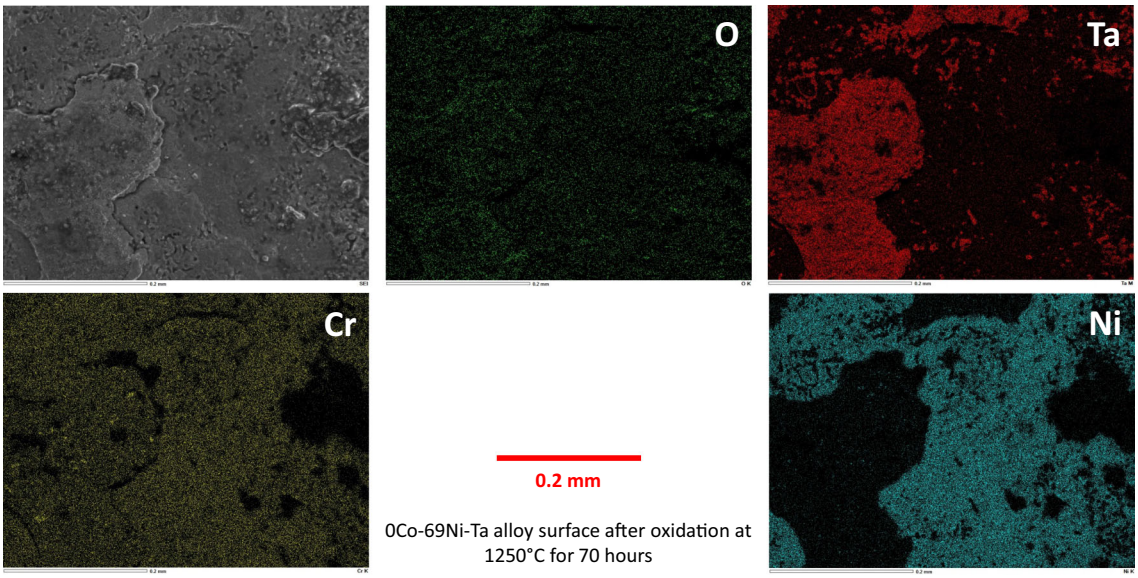

Fig. 9—Example of a local X-ray map of the oxidized surface of the alloys (here: the cobalt-free Ni-based alloy 0Co-69Ni-Ta).

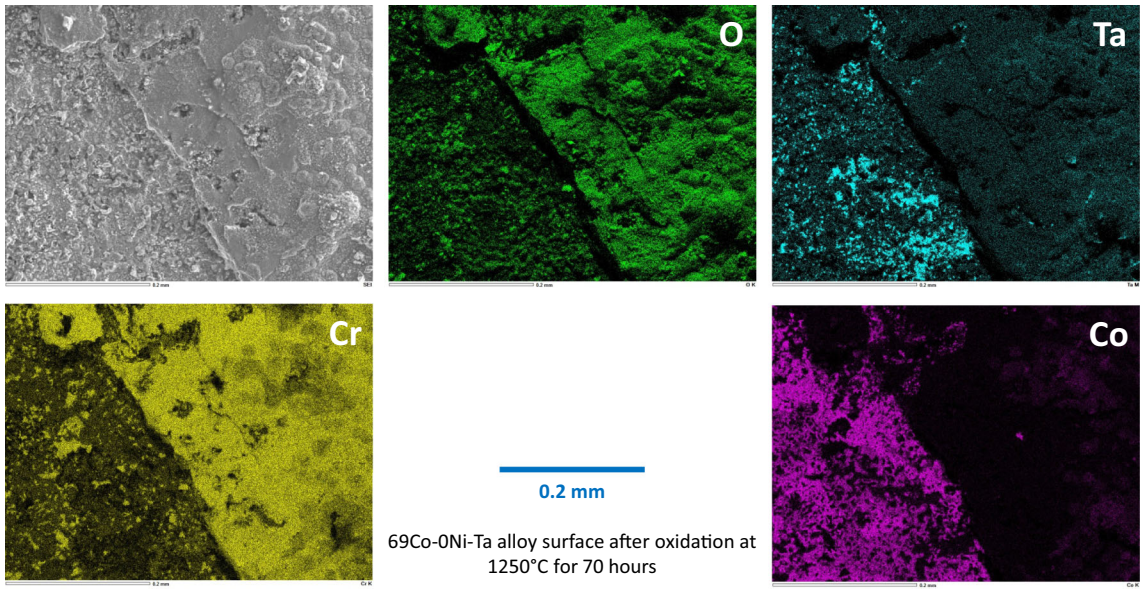

Fig. 10—Example of a local X-ray map of the oxidized surface of the alloys (here: the nickel-free Co-based alloy 69Co-0Ni-Ta).

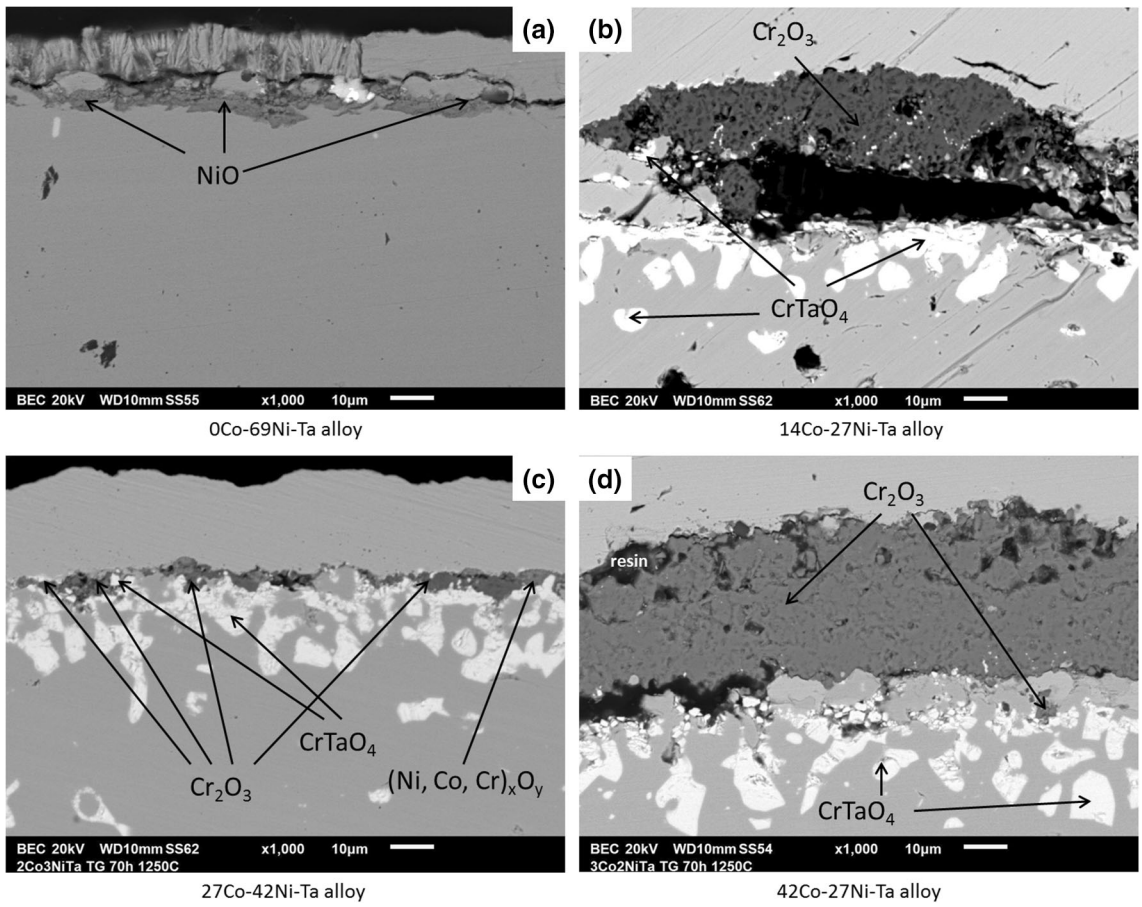

Fig. 11—Detailed view of the oxidized surfaces of the chromia-forming alloys, with identification of the external and internal oxides by spot EDS analysis (the four Ni-richest alloys: (*a*) 0Co-69Ni-Ta, (*b*) 14Co-55Ni-Ta, (*c*) 27Co-42Ni-Ta, and (*d*) 42Co-27Ni-Ta; SEM/BSE, ×1000).

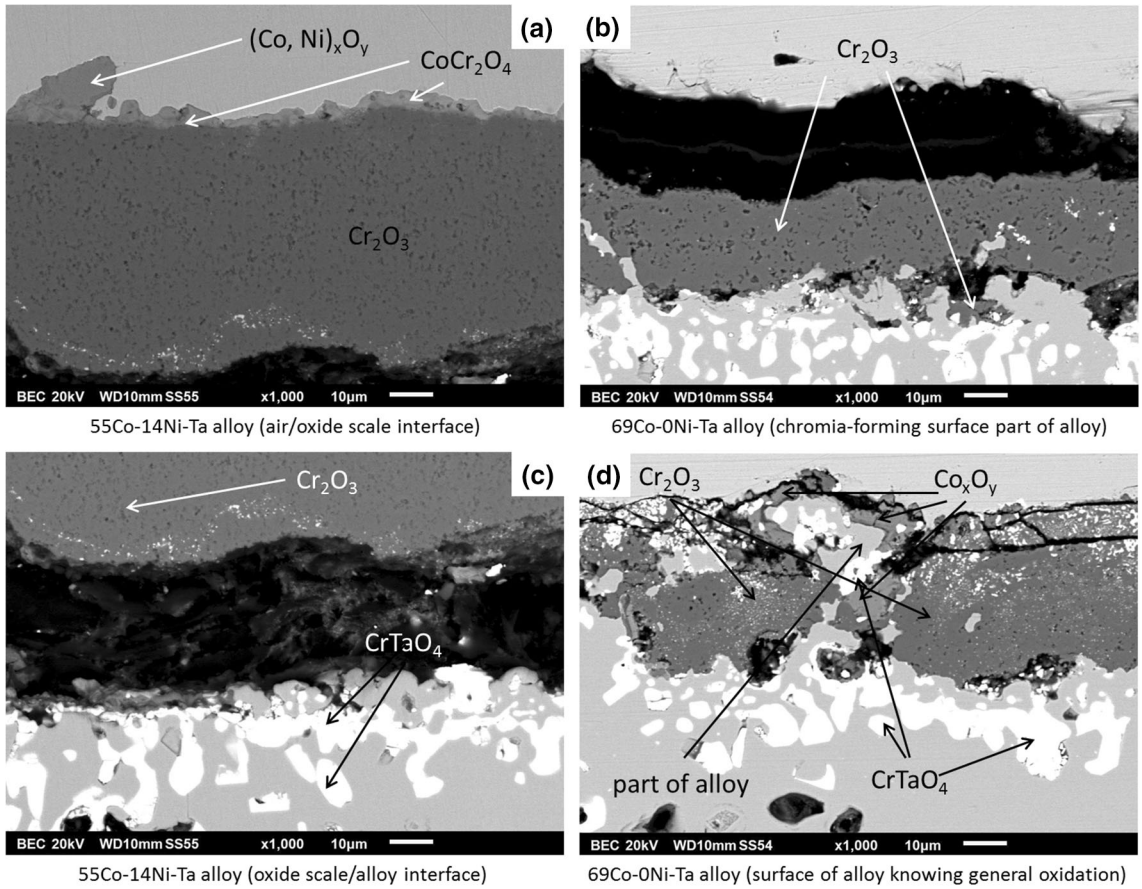

Fig. 12—Detailed view of the oxidized surfaces of the chromia-forming alloys, with identification of the external and internal oxides by spot EDS analysis (the two Co-richest alloys: (*a*, *c*) 55Co-14Ni-Ta and (*b*, *d*) 69Co-0Ni-Ta; SEM/BSE, ×1000).

for the chromium carbides. The natural tendency to minimize the interface area between two solid phases (here matrix and carbide) led here to the loss of the acicular shape of the chromium carbides which became almost round and coarse. The same tendency appeared for the tantalum carbides but results were more limited: they get fractioned but not really coarsened. This can be maybe attributed to a lower interfacial energy for chromium carbides, but more probably to a less easy diffusion of the big Ta atoms in the matrix by comparison to the chromium atoms. Since one can reasonably think that this morphological evolution of the carbides will mechanically weaken the alloys when stressed at high temperature, it is clear that the tantalum carbides are to be favored, at the expense of the chromium carbides. So, in the mechanical field, by comparison to the nickel-richest alloys, the cobalt-richest alloys are advantaged by the absence of chromium carbides and by a greater proportion of tantalum carbides. In addition, the cobalt-richest alloys take benefit from the strength of their matrix. This one is stronger since it is principally made of cobalt.

Concerning oxidation it can be preliminarily noted that none of the studied alloys catastrophically oxidized, despite the very high temperature of exposure to air. All of them developed a continuous external oxide scale, even if this was not obvious due to oxide spallation occurred during the post-isothermal stage cooling.

A second remark that must be done is that, in all cases, carbides have disappeared over a significant depth from the alloy/external scale interface. Chromium, tantalum, and carbon being easy to oxidize, the atoms being very close to the extreme surface of the alloy are oxidized very early. These elements which are now oxidized were previously present in carbides for a part of them, and in solid solution in the matrix for the other part. In the neighborhood of the chromium and tantalum—single or mixed-oxides, the alloy is consequently thermodynamically destabilized since the matrix has become poorer in Cr and in Ta. The same zone is also impoverished in C, oxidized into CO_2 gas that went away outside. Thus, mechanically, this decrease in the local Cr, Ta, and C activities induced two parallel phenomena: 1/diffusion, toward this {Cr, Ta, C}-impoverished outermost zone from the slightly deeper zone (for each element proportionally to both its local concentration gradient and its diffusion coefficient in this metallurgical environment), and also, 2/local change of the microstructure toward the metallurgical state which corresponds to the new local chemical

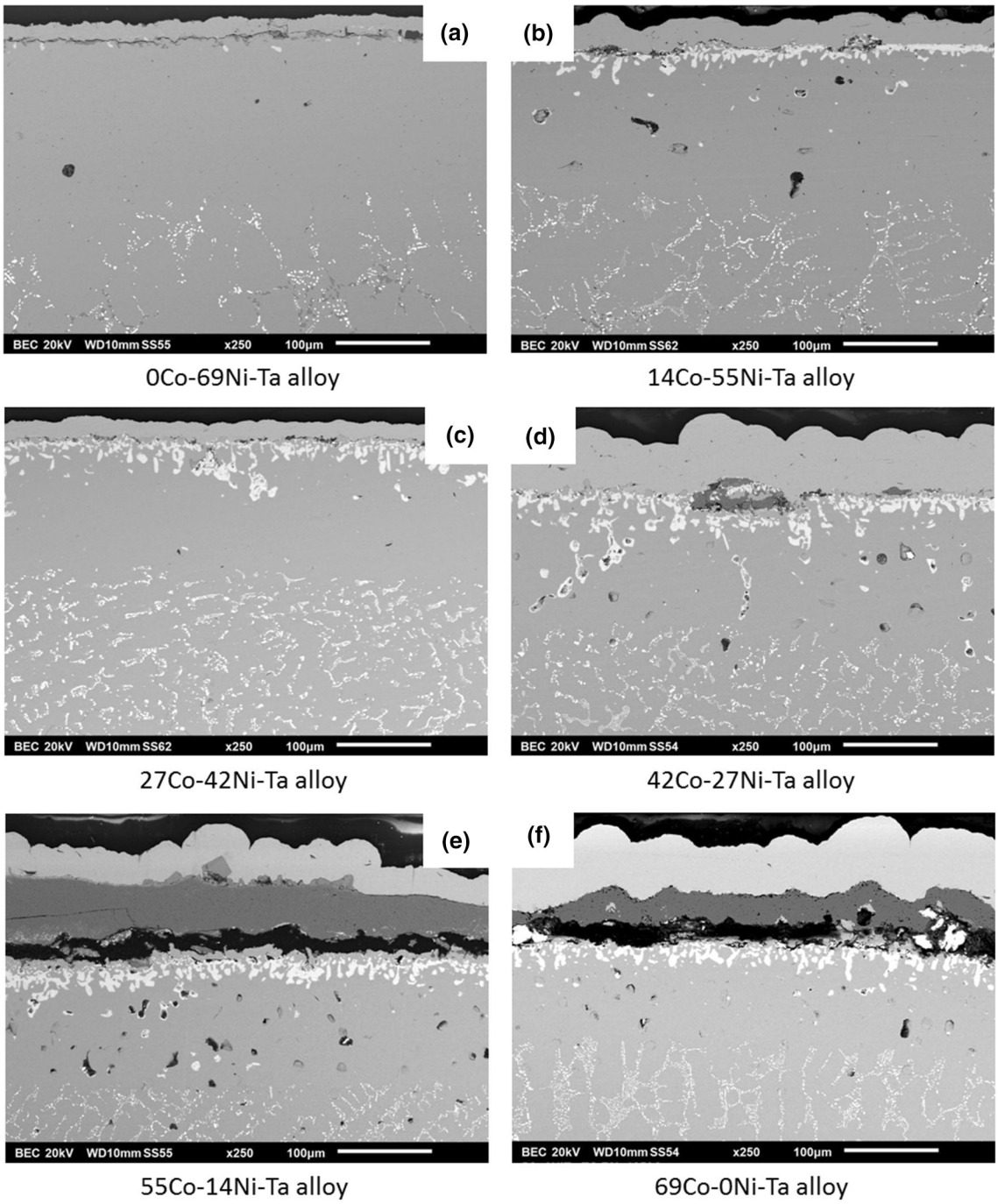

Fig. 13—View of the subsurfaces of all the alloys after oxidation (SEM/BSE, ×250) (*a*) 0Co-69Ni-Ta, (*b*) 14Co-55Ni-Ta, (*c*) 27Co-42Ni-Ta, (*d*) 42Co-27Ni-Ta, (*e*) 55Co-14Ni-Ta, (*f*) 69Co-0Ni-Ta.

composition of the alloy (to be clear: dissociation of a part of the local carbides*,** in order to re-enrich matrix in Cr and C (*from the dissolving chromium carbides of the Ni-richest alloy) and in Ta and C (**from the dissolving TaC for all alloys of this work). Since the oxidation progress goes on, more and more chromium, tantalum, and carbon are oxidized and thus more and more Cr, Ta, and C atoms diffuse from deeper and deeper alloy zones. And in parallel, Cr, Ta, and C are released by the dissolution of the carbides which are

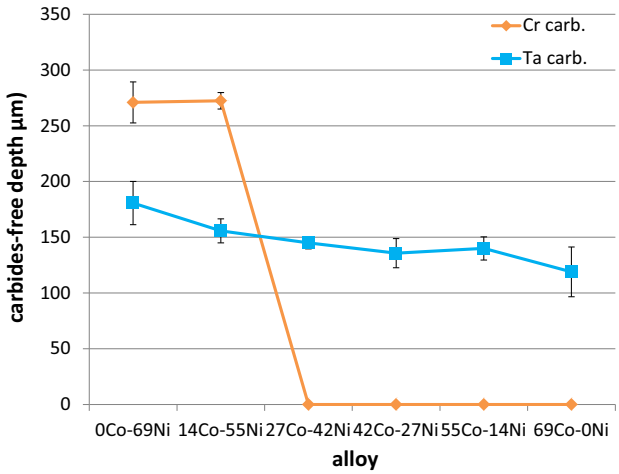

Fig. 14—Evolution, *vs* the Ni/Co ratio, of the depth of disappearance of the chromium carbides and of the one of the tantalum carbides.

initially the closest to the alloy extreme surface, and after their total disappearance (more probably also simultaneously with the end of dissolution of these first carbides to be affected), by the start of dissolution of the carbides located just a little deeper. With time this local {Cr, Ta, C}-impoverishment of the alloy and this carbide dissolution both propagate deeper and deeper in the alloy, farer and farer from the oxidation front. After the rather long duration of the present oxidation tests (17 hours) and for the particularly high exposure temperature (1250 °C), this led here to rather great depths of {Cr, Ta, C}-depletion and of carbide disappearance. This was seen above on the concentration profiles and on the low magnification cross-sectional SEM/BSE micrographs, respectively.

About the problem of oxide scale loss during cooling, it can be noted that this is for the nickel-richest alloys that the spallation phenomenon was the most intensive. This may be attributed to a possible higher participation of tantalum in the oxide formation in the innermost part of the external scale in the case of the cobalt-free nickel-based alloy, and maybe also for the second Ni-richest alloy. For the former one (0Co-69Ni-Ta alloy), no internal oxidation was noticed in the outermost part of alloy, although all carbides, including TaC, have disappeared in the subsurface from a great depth. The corresponding tantalum initially present as carbides has necessarily been oxidized, as external oxide since no internal oxide has appeared. In the case of the following alloy (14Co-55Ni-Ta), which also left its carbides over a slightly lower depth than the preceding alloy, some $CrTaO_4$ are present over a small depth, lower than for the other alloys containing more cobalt. It can be thought that tantalum maybe diffused easier in the matrix of the two nickel-richest (flat Ta content profile) alloys than in the other alloys richer in cobalt (existing Ta content gradient). This led to localize the formation of the corresponding oxides directly on the oxidation front. This is maybe the formation of many $CrTaO_4$ oxides at this location that harmed the adhesion of chromia on the metallic substrate. For the other alloys, which contain more cobalt or are based on this element rather than on nickel, a slower volume diffusion of Cr and Ta, through the matrix toward the oxidation front, may allow a little inwards diffusion of oxygen and privileged Ta diffusion along the interdendritic boundaries. Therefore, $CrTaO_4$ formed at their meeting point in the interdendritic spaces close to the alloy surface. They are thus observed a little deeper in the subsurface for the alloys with significant content in cobalt. For these alloys containing cobalt, $CrTaO_4$ maybe thus less deleterious for the scale adhesion on alloy, with as consequence less oxide spallation at cooling for a same cooling rate.

According to the observations with the SEM in SE mode, the external oxide scales were well covering the Co-rich samples and XRD runs as well as EDS measurements allowed characterizing the complex structures of the external scale formed over their surfaces. This was also true for the cross-sectional SEM observations and EDS measurements. These external oxide scales were constituted, not only of chromia and $CrTaO_4$, but also of $(Co,Ni)Cr_2O_4/CoCr_2O_4$ spinels and (Co,Ni)O/CoO oxides. This demonstrates a behavior not wholly chromia-forming, and even the imminence of catastrophic oxidation, at least locally. This is confirmed by rather irregular alloy/scale interfaces here and there for the cobalt, richest alloys. This is in agreement with the Cr contents particularly low in extreme surface by comparison with the nickel-richest alloys at the same location.

V. CONCLUSION

1250 °C is a very high temperature for nickel-based and cobalt-based superalloys, and particularly for the alloys studied in this work which contain eutectic compounds involving carbides. For such elevated temperature, 70 hours (*i.e.,* three days), duration very short for superalloys used at 800 °C, 1000 °C, or even 1100 °C, represents a long duration in terms of oxidation solicitation as well as of morphological stability of the carbides. Despite these severe conditions, the Ni-rich versions rather well behaved in oxidation resistance. The

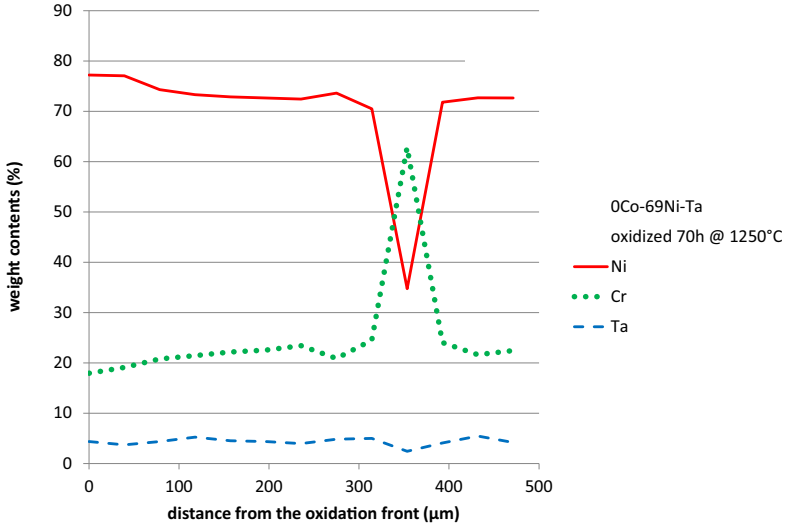

(a)

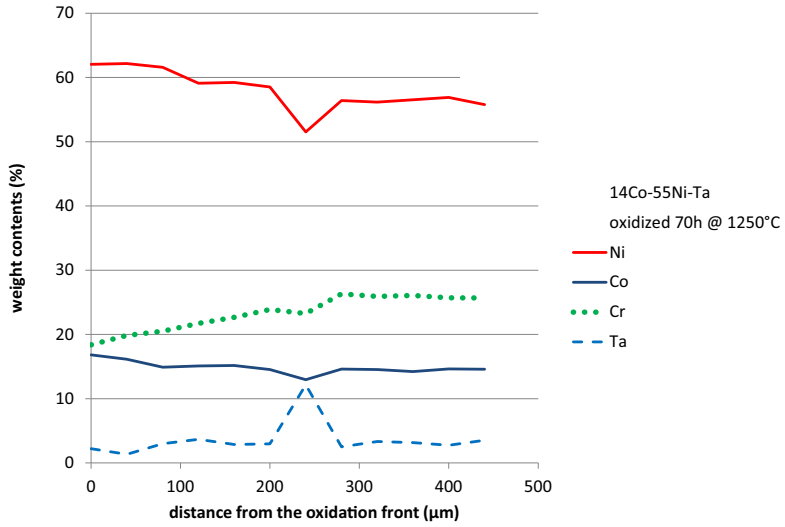

(b)

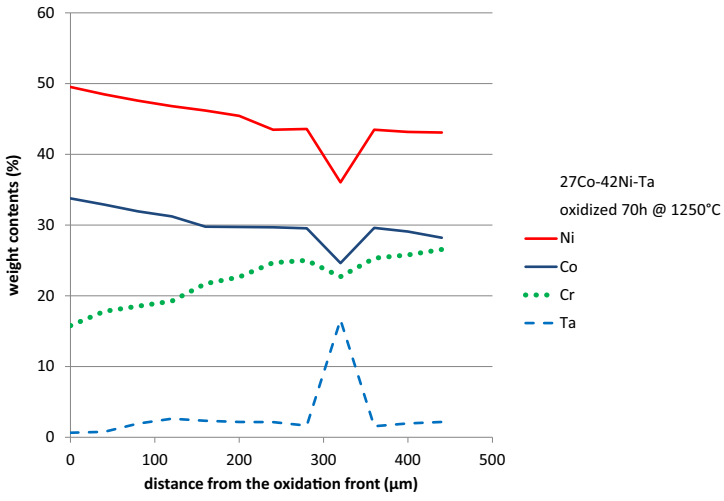

(c)

Fig. 15—Concentration profiles of the main elements over a depth of 500 μm for the three Ni-richest alloys after oxidation: (*a*) 0Co-69Ni-Ta, (*b*) 14Co-55Ni-Ta and (*c*) 27Co-42Ni-Ta.

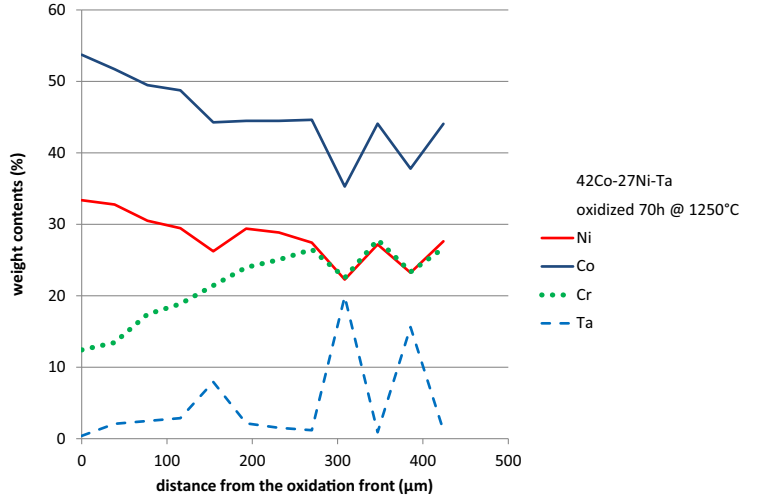

(a)

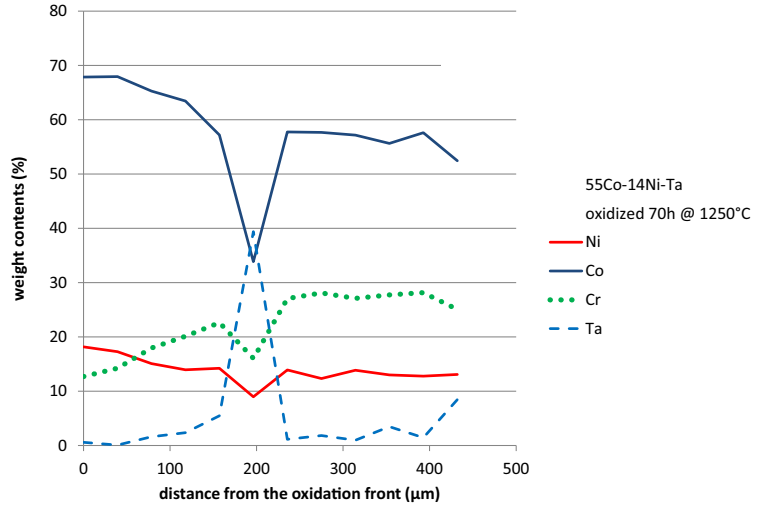

(b)

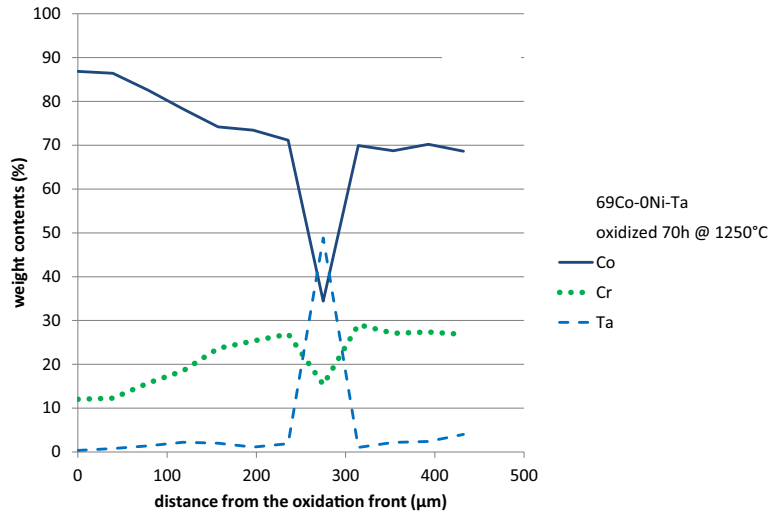

(c)

Fig. 16—Concentration profiles of the main elements over a depth of 500 μm for the three Co-richest alloys after oxidation: (*a*) 42Co-27Ni-Ta, (*b*) 55Co-14Ni-Ta and (*c*) 69Co-0Ni-Ta.

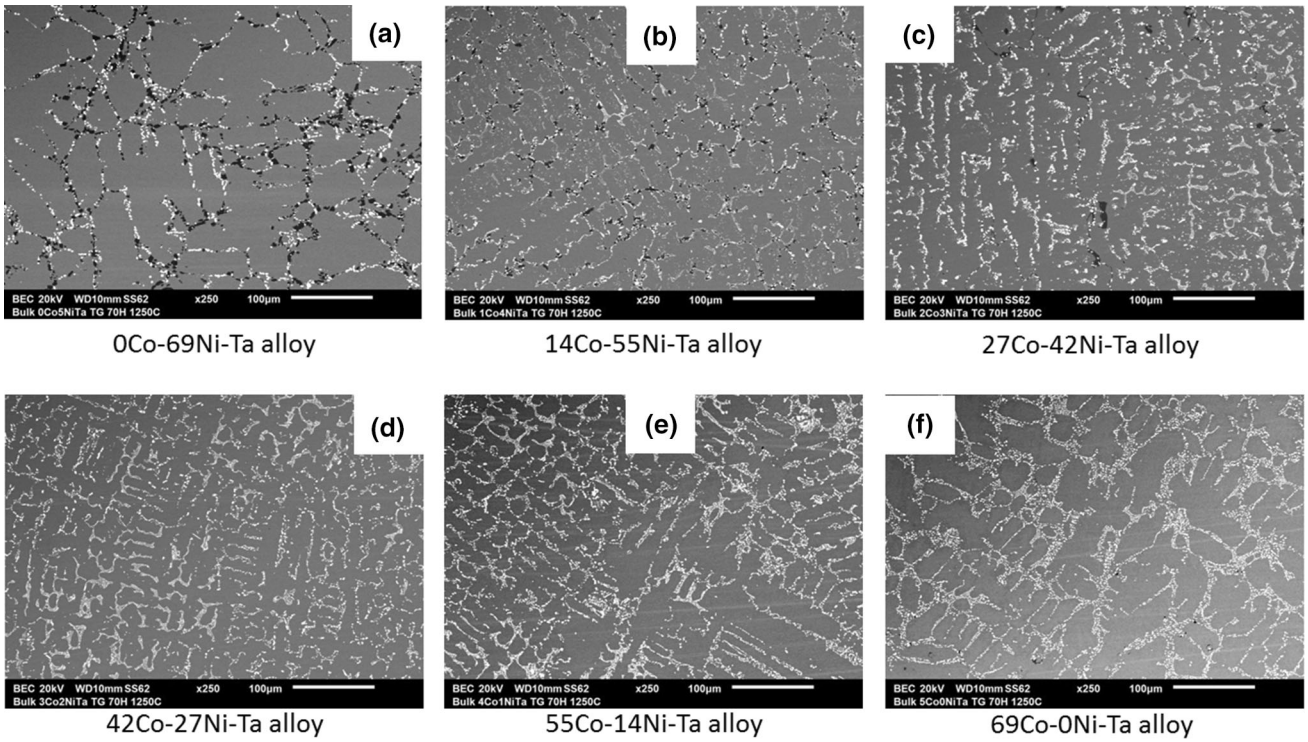

Fig. 17—The microstructures of the six alloys of the study, after 70 h at 1250 °C (SEM/BSE, general view: ×250); (*a*) 0Co-69Ni-Ta, (*b*) 14Co-55Ni-Ta, (*c*) 27Co-42Ni-Ta, (*d*) 42Co-27Ni-Ta, (*e*) 55Co-14Ni-Ta, (*f*) 69Co-0Ni-Ta.

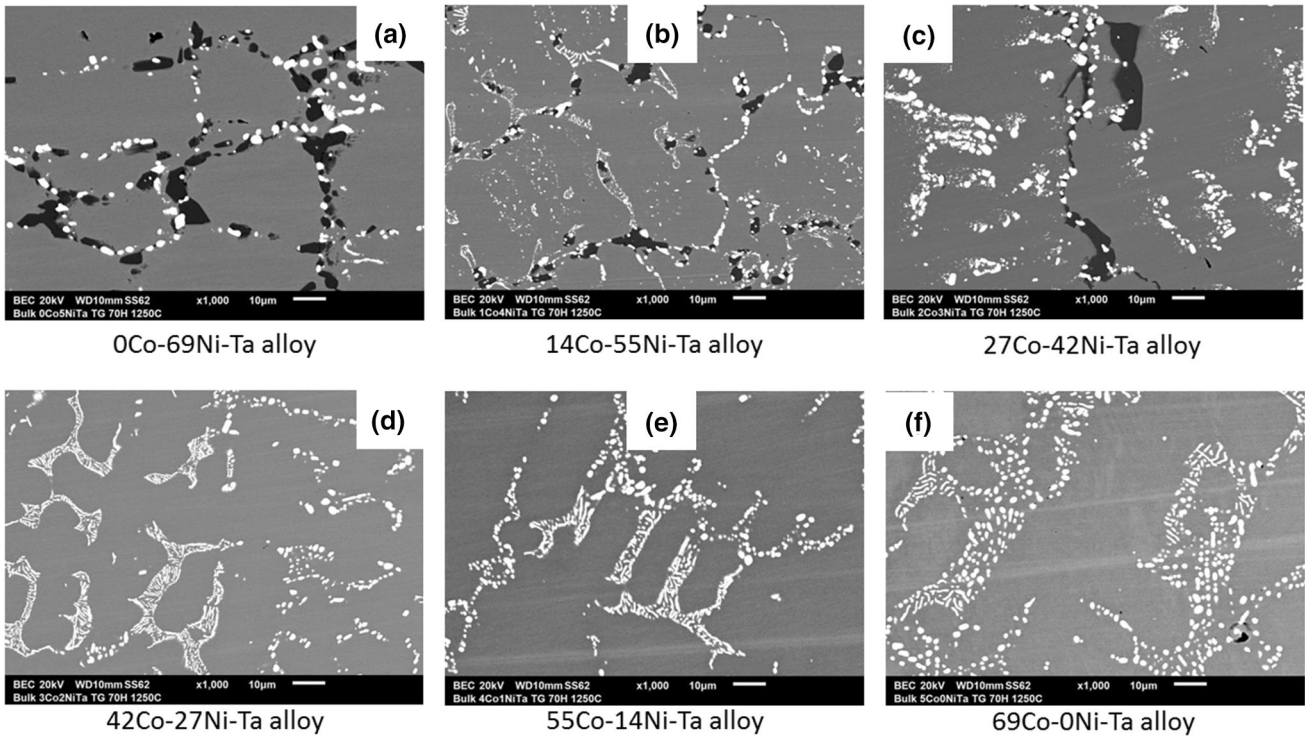

Fig. 18—The microstructures of the six alloys of the study, after 70 h at 1250 °C (SEM/BSE, detailed view: ×1000); (*a*) 0Co-69Ni-Ta, (*b*) 14Co-55Ni-Ta, (*c*) 27Co-42Ni-Ta, (*d*) 42Co-27Ni-Ta, (*e*) 55Co-14Ni-Ta, (*f*) 69Co-0Ni-Ta.

cobalt-richest alloys were much more impoverished in chromium and seemed to be ready to start being much more damaged by oxidation. The behavior dependence on the Co/Ni ratio maybe inversed concerning the mechanical properties at high temperature since the TaC carbides, single carbide existing in the cobalt-richest alloys and, in this way, with the greatest volume fractions for a same given carbon content, were less morphologically deteriorated than the global carbide population in the nickel-richest alloys. All these alloys seem to be exploitable at 1250 °C in air for not too long periods but some of them are more interesting than the others following the oxidation/creep combinations of required properties.

ACKNOWLEDGMENT

The authors wish to thank Mr. Lionel Aranda for his help for the oxidation tests.

REFERENCES

1. C.T. Sims and W.C. Hagel: *The Superalloys*, Wiley, New York, 1972.
2. P. Kofstad: *High Temperature Corrosion*, Elsevier Applied Science, London, 1988.
3. E.F. Bradley: *Superalloys: A Technical Guide*, ASM International, Metals Park, 1988.
4. M. Durand-Charre: *The Microstructure of Superalloys*, CRC Press, Boca Raton, 1997.
5. M.J. Donachie and S.J. Donachie: *Superalloys—A Technical Guide*, 2nd ed., ASM International, Materials Park, 2002.
6. D.J. Young: *High Temperature Oxidation and Corrosion of Metals*, Elsevier Corrosion Series, Amsterdam, 2008.
7. W. Sun, X. Qin, J. Guo, L. Lou, and L. Zhou: *Mater. Des.*, 2015, vol. 69, pp. 81–88.
8. L. Liu, F. Sommer, and H.Z. Fu: *Scr. Metall. Mater.*, 1994, vol. 30, pp. 587–91.
9. L. Zheng, S. Li, C. Xiao, D. Tang, and C. Gu: *Key Eng. Mater.*, 2007, vols. 353–358, pp. 507–10.
10. T. Zhao, D. Wang, J. Zhang, G. Chen, and L.H. Lou: *J. Mater. Sci. Technol.*, 2009, vol. 25, pp. 361–64.
11. P. Berthod: *Adv. Mater. Sci. Eng.*, 2017, Article ID 4145369, https://doi.org/10.1155/2017/4145369.
12. W.H. Jiang, X.D. Yao, H.R. Guan, and Z.Q. Hu: *Acta Metall. Sin. (English Letters)*, 1999, vol. 12, pp. 155–59.
13. B.J. Piearcey and R.W. Smashey: *Trans. Metall. Soc. AIME*, 1967, vol. 239, pp. 451–57.
14. X.Z. Qin, J.T. Guo, C. Yuan, J.S. Hou, and H.Q. Ye: *Mater. Sci. Forum*, 2007, vols. 546–549, pp. 1301–04.
15. J.M. Drapier, P. Viatour, and D. Coutsouradis: *Cobalt (English Edition)*, 1971, vol. 52, pp. 147–55.
16. P. Berthod: *J. Alloys Compd.*, 2009, vol. 481, pp. 746–54.
17. P. Berthod and E. Conrath: *Mater. High Temp.*, 2014, vol. 31, pp. 266–73.
18. P. Berthod and E. Conrath: *Mater. Chem. Phys.*, 2014, vol. 143, pp. 1139–48.
19. E. Conrath and P. Berthod: *Int. J. Mater. Res. (formerly Z. Metallkd.)*, 2014, vol. 105, pp. 717–24.
20. P. Berthod and E. Conrath: *Mater. Sci. Technol.*, 2015, vol. 31, pp. 1764–72.
21. D.A. Woodford: *Metall. Trans. A: Phys. Metall. Mater. Sci.*, 1977, vol. 8A, pp. 639–50.
22. E.R. Buchanan and L.A. Tarshis: *Metall. Trans.*, 1974, vol. 5, pp. 1413–22.
23. Z. Opiekun: *J. Mater. Sci.*, 1987, vol. 22, pp. 1547–56.
24. P. Berthod, S. Michon, L. Aranda, S. Mathieu, and J.C. Gachon: *Comput. Coupling Phase Diagr. Thermochem.*, 2003, vol. 27, pp. 353–59.
25. P. Berthod, J.-L. Bernard, and C. Liébaut: *International Patent*, 2001, WO 01/90429 A1.25.